Int. J. Heat Mass Transfer. Vol. 27, No. 8, pp. 1251–1259, 1984
Printed in Great Britain

0017 9310/84 $3.00 + 0.00
Pergamon Press Ltd.

SOME ASPECTS OF TURBULENT HEAT TRANSFER IN ACCELERATED FLOWS ON PERMEABLE SURFACES

P. S. ROGANOV, V. P. ZABOLOTSKY, E. V. SHISHOV and A. I. LEONTIEV
N. E. Bauman Higher Technical College, 107005, Moscow, U.S.S.R.

(*Received* 18 *May* 1983)

Abstract—The results of an experimental investigation of the structure and processes of turbulent transfer in an accelerated boundary layer on a permeable surface are presented. Possible ways of modelling the transport equation for a turbulent heat flux are analysed. Emphasis is given to the modelling of pressure–temperature correlations.

NOMENCLATURE

a	thermal diffusivity [W m^{-1} K^{-1}]
b	injection parameter, $\rho V_m/\rho U_\infty$
$C_{i_1}, C_{i_2}, C_{i_3}$	dimensionless constants
C_f	local friction coefficient
e	kinetic energy of turbulence [m^2 s^{-2}]
K	acceleration parameter, $(\nu/U_\infty^2)(dU_\infty/dx)$
K_w	roughness size
p'	pressure fluctuations
Pr	Prandtl number
Pr_T	turbulent Prandtl number
$R_{\overline{uv}}, R_{\overline{v\theta}}$	correlation coefficients
Re_T^{**}	Reynolds number, $U_\infty \delta_T^{**}/\nu$
T	mean temperature [K]
U, V	mean velocity components in the x- and y-directions [m s^{-1}]
u', v', w'	fluctuational velocity components [m s^{-1}]
U_τ	dynamic velocity [m s^{-1}]
St	Stanton number
X, Y	longitudinal and transverse coordinates, respectively [m].

Greek symbols

δ	boundary layer thickness [m]
δ_T	thermal boundary layer thickness [m]
δ^{**}	displacement thickness [m]
δ_T^{**}	energy loss thickness [m]
ρ	density [kg m^{-3}]
θ'	temperature fluctuations [K]
ν	viscosity [m^2 s^{-1}]
ε	turbulent energy dissipation [m^2 s^{-3}]
ε_θ	'dissipation' of temperature fluctuations [K^2 s^{-1}].

Subscripts

∞	in free stream
w	at the wall.

AT PRESENT, the development and further refinement of the models which would accurately describe the transport of turbulent heat flux involve a fair number of difficulties residing mainly in the lack of reliable experimental data on the fluctuational structure of thermal and dynamic boundary layers under the conditions when the analogy between the processes of momentum and heat transfer breaks down substantially.

As is known [1, 2], such flows include a highly accelerated turbulent boundary layer on a permeable surface, i.e. the case which is rather frequently encountered in modern power engineering equipment when providing thermal protection for especially stressed elements of the surface of operating channels.

This paper presents the results of an experimental investigation of the fluctuational structure of thermal and velocity boundary layers, developing on a porous plate under the action of high longitudinal negative pressure gradients in the presence of injection, the analysis of which has made it possible to verify experimentally the validity of different hypotheses used to approximate the correlations involving pressure fluctuations and to suggest the transport equation for a turbulent heat flux, which physically correctly models the processes of transfer under the conditions of substantial violation of the Reynolds analogy.

The experimental facility used was a subsonic open wind tunnel the schematic diagram and basic dimensions of which are given in ref. [3].

The studied accelerated turbulent boundary layer was developed on a porous plate made of polymethyl acrylate powder by preheat molding. A segmented system of air injection allowed the provision of different rates of injection along the length of the plate. Small powder grain dimensions ($\sim 50\ \mu$m) made it possible to obtain a hydrodynamically smooth surface according to the estimate made by the Nikuradze criterion

$$\frac{U_\tau K_w}{\nu} < 5.$$

The heating of the test section on the plate was carried out by injection of warm air. The scheme and the arrangement of measuring cross-sections are shown in Fig. 1. A more detailed description of these is given in ref. [3].

The measurements were made by the 'hot wire' technique with the aid of DISA 55-M hot-wire

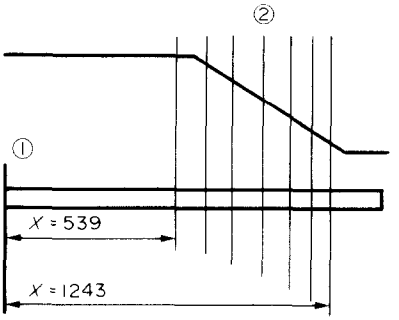

FIG. 1. Schematic diagram of the test section: (1) beginning of porous plate; (2) location of measuring cross-sections.

anemometers. The standard one-filament probes and a combined three-filament probe with a filament thickness of 2.5 μm were used. The specificity of operation in nonisothermal flows was taken into account by the method described in ref. [4]. The heat transfer and surface friction coefficients were determined from the slope of the temperature and velocity profiles in the wall region; the readings of the thermoanemometer, which operated in the constant-temperature regime, were corrected for the wall cooling effect [5]. In measuring the dissipative derivatives of temperature fluctuations, the amplitude–frequency hot-wire response was corrected with account for the thermal lag of the thermoanemometer probe filament operating in the constant-current regime.

The main parameters and integral characteristics of the boundary layer investigated are listed in Table 1. The integral characteristics were obtained as a result of processing the velocity and temperature profiles measured at the cross-sections mentioned and are given in Tables 2 and 3, respectively. Moreover, at section No. 6 ($X = 1143$ mm), where the studied boundary layer and its properties approaches the asymptotic boundary layer; detailed measurements of fluctuational characteristics were made, the results of which are given in Table 4.

A comparison of the present experimental data with the results of investigations carried out with an impervious plate at the same acceleration parameter [6] has shown that injection turbulizes the flow in the outer portion of the boundary layer. Under these conditions, the flow in the outer part of the boundary layer becomes more isotropic, and therefore the production due to normal stresses ceases to play the role of the 'sink' in the total production of turbulence energy (Fig. 2) [6]

$$\text{Production} = -\overline{u'v'}\frac{\partial U}{\partial y} - (\overline{u'^2} - \overline{v'^2})\frac{\mathrm{d}U}{\mathrm{d}x}.$$

A characteristic feature of highly accelerated turbulent flows with injection is a nonmonotonic nature of the mixing length distribution (Fig. 3), which is indicative of a strong deformation of wall flows in the confusor region. Therefore, the allowance for the effect of the longitudinal pressure gradient and injection on the mixing length distribution, assumed in a number of calculation methods, can at best be made only in the region adjacent to the wall.

An important feature of highly accelerated 'laminarized' flows is a substantial infringement of the conservative nature of the 'standard' heat transfer law

$$St = 0.0144 Re_{\mathrm{T}}^{**\,-0.25}.$$

It is known that acceleration and injection separately lead to a decrease in the respective values of St. However, as is seen from Fig. 4, the combined effect of acceleration and injection, even though it leads to a decrease in the values of St, is yet not so pronounced and does not obey the superposition principle.

A complex nature of the combined effect of acceleration and injection on heat transfer is explained by the fact that, on the one hand, the injection, while turbulizing the wall region of the boundary layer, decreases the relative thickness of a viscous sublayer (Fig. 5) and enhances heat transfer and, on the other hand, both the acceleration and injection decrease the level of turbulent heat flux naturally leading to the inverse effect.

An additional decrease of the turbulent heat flux level on a permeable plate (Fig. 6) is due to the fact that in the wall region of the boundary layer the interaction of the opposite normal velocity components of the injected air

Table 1. Basic parameters of the flow

Number of cross-section	X† (mm)	U_∞ (m s^{-1})	ΔT_∞ (K)	δ (mm)	δ_{T} (mm)	δ^{**} (mm)	δ_{T}^{**}	C_{f} $\times 10^3$	St_x $\times 10^3$
1	539	6.95	7.22	23.83	25.75	3.14	4.87	2.73	1.75
2	662	7.25	7.21	25.48	25.32	3.28	5.06	2.97	1.49
3	747	7.70	7.19	22.41	23.57	2.79	5.28	3.11	1.22
4	947	9.75	8.81	19.61	20.35	1.77	3.80	3.48	1.26
5	975	10.25	9.50	19.58	20.24	1.74	3.68	3.48	1.29
6	1143	14.24	13.01	16.52	19.06	1.28	2.15	3.64	1.51
7	1248	19.11	17.20	10.08	16.86	0.84	1.72	3.56	1.63

†X is the distance from the beginning of the porous plate.

Table 2. Velocity profiles (y is the distance along the normal to the surface)

Y (mm)	U_1 (m s^{-1})	U_2 (m s^{-1})	U_3 (m s^{-1})	U_4 (m s^{-1})	U_5 (m s^{-1})	U_6 (m s^{-1})	U_7 (m s^{-1})
0.00	0.00	0.00	0.00	0.00	0.00	0.00	0.00
0.05	0.22	0.26	0.31	0.56	0.62	1.24	2.18
0.10	0.44	0.53	0.62	1.11	1.23	2.47	3.94
0.15	0.66	0.79	0.93	1.67	1.85	3.63	5.34
0.20	0.88	1.05	1.24	2.18	2.38	4.56	6.46
0.25	1.11	1.31	1.54	2.65	2.86	5.29	7.36
0.30	1.32	1.54	1.82	3.08	3.29	5.88	8.08
0.40	1.70	1.95	2.30	3.81	4.03	6.76	9.21
0.50	2.03	2.29	2.69	4.41	4.64	7.46	10.09
0.60	2.31	2.56	3.01	4.89	5.13	8.03	10.85
0.70	2.55	2.78	3.27	5.28	5.54	8.52	11.50
0.80	2.75	2.97	3.48	5.61	5.88	8.93	12.06
1.00	3.05	3.28	3.82	6.11	6.40	9.61	12.96
1.50	3.54	3.74	4.34	6.79	7.13	10.63	14.41
2.00	3.81	4.01	4.64	7.15	7.51	11.14	15.29
2.50	3.96	4.21	4.86	7.39	7.76	11.51	15.96
3.00	4.08	4.37	5.03	7.57	7.96	11.80	16.53
3.50	4.19	4.52	5.17	7.74	8.13	12.04	17.03
4.00	4.32	4.66	5.30	7.88	8.29	12.28	17.44
4.50	4.44	4.79	5.42	8.02	8.43	12.48	17.76
5.00	4.55	4.90	5.52	8.14	8.57	12.65	18.01
6.00	4.77	5.09	5.72	8.36	8.81	12.91	18.33
7.00	4.98	5.27	5.90	8.53	9.00	13.12	18.50
8.00	5.17	5.44	6.07	8.68	9.16	13.30	18.65
9.00	5.35	5.60	6.23	8.82	9.31	13.45	18.81
10.00	5.50	5.75	6.38	8.95	9.44	13.58	18.97
11.00	5.65	5.89	6.52	9.06	9.57	13.70	19.11
12.00	5.79	6.03	6.65	9.17	9.69	13.80	
13.00	5.94	6.16	6.78	9.27	9.80	13.89	
14.00	6.08	6.28	6.91	9.36	9.89	13.97	
15.00	6.22	6.40	7.03	9.45	9.98	14.06	
16.00	6.34	6.51	7.15	9.52	10.05	14.13	
18.00	6.56	6.71	7.37	9.64	10.15	14.24	
20.00	6.73	6.89	7.55	9.72	10.21		
22.00	6.85	7.04	7.65	9.75	10.24		
24.00	6.92	7.16	7.70		10.25		
26.00	6.95	7.24					
28.00	6.96	7.27					

and of the transverse flow, attributable to the two-dimensional (2-D) nature of the flow in the boundary layer, causes the appearance of the transverse velocity fluctuation components that are less correlated, due to different generation mechanisms, with both the longitudinal velocity fluctuations and temperature fluctuations. The validity of this assumption is proved by the analysis of the distribution of correlation coefficients $R_{\overline{uv}}$ and $R_{\overline{v\theta}}$ (Fig. 7).

Thus, the injection, which leads to a decrease in the heat transfer coefficients under the conditions of nongradient flow, may lead, at a particular combi-

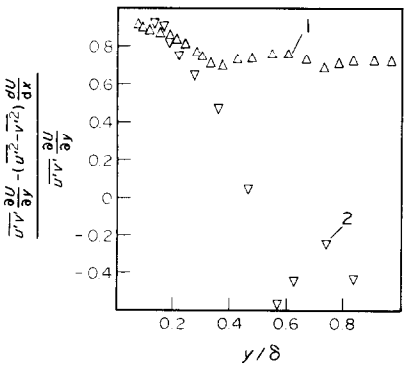

FIG. 2. The role of 'normal components' in the production of turbulent energy: (1) $K = 2.35 \times 10^{-6}$, $b = 0.0033$; (2) $K = 2.35 \times 10^{-6}$, $b = 0$.

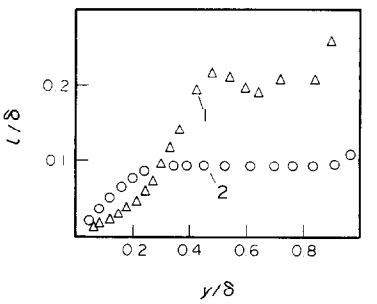

FIG. 3. 'Mixing length' distribution: (1) $K = 2.35 \times 10^{-6}$, $b = 0.0033$; (2) $K = 0$, $b = 0$.

Table 3. Temperature profiles (y is the distance along the normal to the surface: $T^* = T_w - T$)

Y (mm)	T_1^* (K)	T_2^* (K)	T_3^* (K)	T_4^* (K)	T_5^* (K)	T_6^* (K)	T_7^* (K)
0.00	0.00	0.00	0.00	0.00	0.00	0.00	0.00
0.05	0.19	0.17	0.15	0.23	0.27	0.57	1.07
0.10	0.38	0.34	0.29	0.46	0.53	1.11	2.11
0.15	0.57	0.51	0.44	0.69	0.79	1.70	3.12
0.20	0.76	0.68	0.59	0.92	1.04	2.30	4.08
0.25	0.97	0.83	0.74	1.14	1.28	2.87	4.89
0.30	1.13	0.94	0.90	1.36	1.49	3.47	5.35
0.40	1.43	1.16	1.16	1.69	1.83	4.66	6.06
0.50	1.63	1.34	1.31	1.97	2.13	5.71	6.67
0.60	1.79	1.50	1.38	2.22	2.41	6.56	7.22
0.70	1.94	1.64	1.47	2.46	2.67	7.16	7.72
0.80	2.09	1.76	1.59	2.67	2.89	7.55	8.16
1.00	2.32	1.97	1.73	3.01	3.26	8.00	8.89
1.50	2.64	2.34	2.12	3.63	3.94	8.85	10.31
2.00	2.84	2.64	2.39	4.12	4.47	9.23	11.42
2.50	3.00	2.87	2.63	4.51	4.92	9.51	12.28
3.00	3.15	3.07	2.85	4.84	5.32	9.73	12.95
3.50	3.29	3.23	3.04	5.11	5.65	9.94	13.48
4.00	3.42	3.39	3.20	5.35	5.94	10.14	13.93
4.50	3.54	3.53	3.34	5.55	6.17	10.32	14.31
5.00	3.66	3.67	3.47	5.72	6.36	10.50	14.64
6.00	3.89	3.91	3.74	6.00	6.67	10.80	15.17
7.00	4.09	4.13	4.01	6.25	6.93	11.05	15.58
8.00	4.31	4.34	4.26	6.51	7.18	11.28	15.92
9.00	4.53	4.54	4.48	6.76	7.40	11.47	16.19
10.00	4.76	4.75	4.70	6.99	7.62	11.66	16.40
11.00	5.00	4.95	4.90	7.19	7.83	11.83	16.56
12.00	5.24	5.15	5.11	7.38	8.02	12.00	16.69
13.00	5.47	5.35	5.31	7.57	8.21	12.15	16.79
14.00	5.70	5.54	5.52	7.77	8.40	12.31	16.88
15.00	5.91	5.73	5.73	7.96	8.60	12.46	16.96
16.00	6.11	5.91	5.95	8.14	8.79	12.59	17.04
18.00	6.45	6.24	6.37	8.49	9.16	12.84	17.20
20.00	6.69	6.55	6.74	8.73	9.43	13.02	
22.00	6.82	6.84	7.03	8.81	9.50		
24.00	6.93	7.07	7.19				
26.00	7.22	7.21					
28.00	7.77						

nation with the longitudinal acceleration, to a relative increase in heat transfer.

Consequently, under the conditions considered the use of the transport equation for turbulent heat flux transfer, which accounts for the effect of boundary conditions on the processes of turbulent transfer, is physically reasonable. This idea is also confirmed by the analysis of experimental distributions of Pr_T numbers presented in Fig. 8, which testify to a strong dependence of the distribution of Pr_T numbers on the boundary conditions.

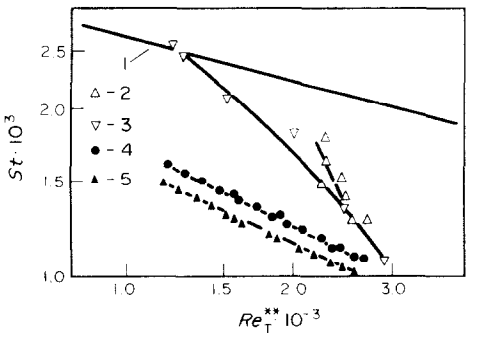

FIG. 4. Distribution of St numbers: (1) $St = 0.0144 Re_T^{**-0.25}$; (2) $K = 2.35 \times 10^{-6}$, $b = 0.0033$; (3) $K = 2.35 \times 10^{-6}$, $b = 0$; (4) $K = 0$, $b = 0.004$ [2]; (5) $K = 2.6 \times 10^{-6}$, $b = 0.004$ [1].

At section No. 6 of the boundary layer investigated, individual components of the balance equations of turbulent energy transfer, Reynolds stresses, magnitudes of temperature fluctuations and of the rates of turbulent heat flux were determined experimentally. In the case of a steady-state 2-D turbulent boundary layer, these equations can be written as

$$U\frac{\partial e}{\partial x} + V\frac{\partial e}{\partial y} = -\overline{u'v'}\frac{\partial U}{\partial y} - (\overline{u'^2} - \overline{v'^2})\frac{\partial U}{\partial x} - \frac{\partial}{\partial y}\left(\frac{\overline{p'v'}}{\rho} + \overline{ev'}\right) + \varepsilon, \quad (1)$$

$$U\frac{\partial \overline{u'v'}}{\partial x} + V\frac{\partial \overline{u'v'}}{\partial y} = -\overline{v'^2}\frac{\partial U}{\partial y} - \frac{\partial}{\partial y}(\overline{v'^2 u'}) + u'\frac{\overline{\partial p'}}{\partial y} + 6\nu\frac{\overline{\partial p'}}{\partial x} + 6\nu\left(\frac{\overline{\partial u'}}{\partial x}\frac{\overline{\partial v'}}{\partial x}\right), \quad (2)$$

Table 4. Fluctuational characteristics at cross-section No. 6

Y (mm)	$\overline{u'^2}$ ($m^2 s^{-2}$)	$\overline{v'^2}$ ($m^2 s^{-2}$)	$\overline{w'^2}$ ($m^2 s^{-2}$)	$\overline{\theta'^2}$ (K^2)	$\overline{u'v'}$ ($m^2 s^{-2}$)	$\overline{v'\theta'}$ ($K m s^{-1}$)	ε ($m^2 s^{-3}$)	ε_θ ($K^2 s^{-1}$)	$\overline{u'^2v'} \times 10$ ($m^3 s^{-3}$)	$\overline{v'^2u'} \times 10$ ($m^3 s^{-3}$)	$\overline{v'^2\theta'} \times 10$ ($K m^2 s^{-2}$)	$\overline{v'\theta'^2} \times 100$ ($K^2 m s^{-1}$)
1.3	1.192	0.313	0.606	0.497	0.164	0.102	88.70	191.0	0.084	0.351	−0.119	−0.351
1.5	1.062	0.273	0.537	0.497	0.162	0.110	78.05	186.4	0.178	0.341	−0.103	−0.390
2.0	0.855	0.223	0.437	0.497	0.157	0.123	55.08	180.5	0.266	0.276	−0.076	−0.450
2.5	0.712	0.191	0.393	0.497	0.151	0.131	38.27	154.5	0.302	0.235	−0.064	−0.543
3.0	0.619	0.169	0.332	0.497	0.145	0.134	27.68	142.2	0.318	0.208	−0.043	−0.613
3.5	0.518	0.150	0.298	0.497	0.134	0.135	19.53	131.3	0.310	0.188	−0.033	−0.673
4.0	0.444	0.142	0.267	0.497	0.128	0.137	14.24	107.2	0.307	0.179	−0.025	−0.654
4.5	0.378	0.129	0.225	0.490	0.116	0.135	11.84	104.9	0.269	0.152	−0.012	−0.614
5.0	0.331	0.129	0.218	0.484	0.111	0.139	9.740	91.30	0.258	0.139	−0.006	−0.606
5.5	0.289	0.124	0.208	0.481	0.103	0.139	7.920	80.50	0.220	0.109	0	−0.593
6	0.258	0.122	0.198	0.473	0.098	0.139	6.570	73.50	0.182	0.090	0.011	−0.497
7	0.211	0.113	0.183	0.458	0.085	0.133	4.320	61.10	0.107	0.058	0.014	−0.385
8	0.170	0.098	0.145	0.443	0.071	0.124	3.150	53.00	0.062	0.038	0.008	−0.276
9	0.136	0.084	0.116	0.421	0.060	0.113	2.390	46.80	0.036	0.033	0	−0.122
10	0.119	0.075	0.103	0.407	0.053	0.104	1.890	42.50	0.028	0.033	−0.015	0
11	0.106	0.071	0.093	0.379	0.049	0.098	1.660	37.60	0.028	0.035	−0.025	0.252
12	0.100	0.069	0.086	0.364	0.047	0.093	1.450	34.90	0.032	0.040	−0.042	0.479
13	0.094	0.067	0.080	0.338	0.046	0.090	1.314	30.70	0.040	0.043	−0.053	0.610
14	0.083	0.059	0.068	0.300	0.041	0.080	1.200	23.00	0.041	0.043	−0.057	0.730
15	0.078	0.056	0.061	0.276	0.038	0.074	0.970	20.45	0.048	0.045	−0.064	0.880
16	0.067	0.049	0.049	0.242	0.034	0.065	0.860	16.61	0.046	0.041	−0.062	0.910
18	0.058	0.039	0.035	0.176	0.027	0.049	0.760	12.79	0.046	0.041	−0.056	0.770
20	0.045	0.031	0.021	0.120	0.020	0.035	0.440	6.960	0.039	0.034	−0.041	0.470

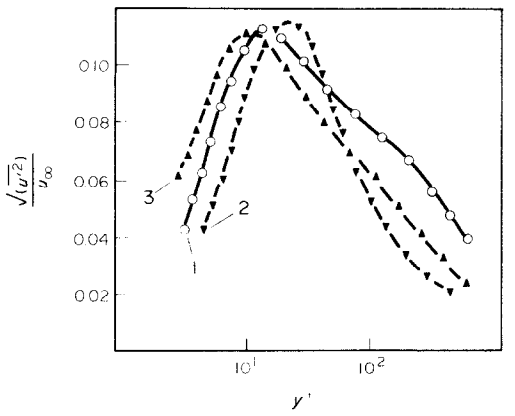

FIG. 5. Distribution of velocity fluctuations in the wall region: (1) $K = 0$, $b = 0$; (2) $K = 2.35 \times 10^{-6}$, $b = 0$; (3) $K = 2.35 \times 10^{-6}$, $b = 0.0033$.

$$U\frac{\partial\overline{\theta'^2}}{\partial x}+V\frac{\partial\overline{\theta'^2}}{\partial y}=-2\overline{u'\theta'}\frac{\partial T}{\partial x}-2\overline{v'\theta'}\frac{\partial T}{\partial y}$$
$$-\frac{\partial}{\partial x}(\overline{u'\theta'^2})-\frac{\partial}{\partial y}(\overline{v'\theta'^2})+a\frac{\partial^2\overline{\theta'^2}}{\partial x^2}+a\frac{\partial^2\overline{\theta'^2}}{\partial y^2}$$
$$-2a\left[\left(\frac{\partial\overline{\theta'}}{\partial x}\right)^2+\left(\frac{\partial\overline{\theta'}}{\partial y}\right)^2+\left(\frac{\partial\overline{\theta'}}{\partial z}\right)^2\right], \quad (3)$$

$$U\frac{\partial\overline{v'\theta'}}{\partial x}+V\frac{\partial\overline{v'\theta'}}{\partial y}=-\left(\overline{u'v'}\frac{\partial T}{\partial x}+\overline{v'^2}\frac{\partial T}{\partial y}\right)$$
$$-\left(\overline{u'\theta'}\frac{\partial V}{\partial x}+\overline{v'\theta'}\frac{\partial V}{\partial y}\right)-\frac{1}{\rho}\frac{\partial\overline{\theta'p'}}{\partial y}-\left(\frac{\partial\overline{u'v'\theta'}}{\partial x}\right.$$
$$\left.+\frac{\partial\overline{v'^2\theta'}}{\partial y}+\frac{1}{\rho}\overline{p'\frac{\partial\theta'}{\partial y}}\right)+a\overline{v'\nabla^2\theta'}+\nu\overline{\theta'\nabla^2 v'}. \quad (4)$$

The technique of experimental determination of the separate terms of these equations is described in detail in refs. [7–10]. The pressure fluctuation terms in equations (2) and (4) were determined as the difference for corresponding equations.

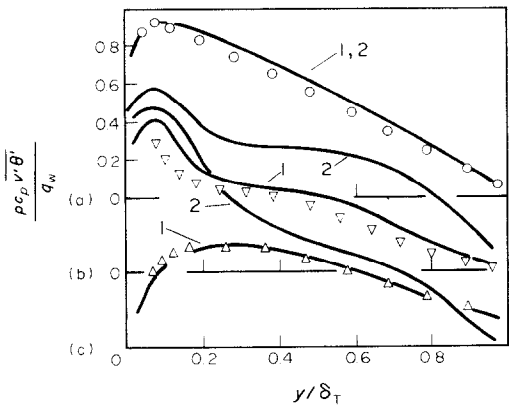

FIG. 6. Distribution of turbulent heat flux: (a) $K = 0$, $b = 0$; (b) $K = 2.35 \times 10^{-6}$, $b = 0$; (c) $K = 2.35 \times 10^{-6}$, $b = 0.0033$; (1) calculation by equation (14); (2) calculation by equation (13).

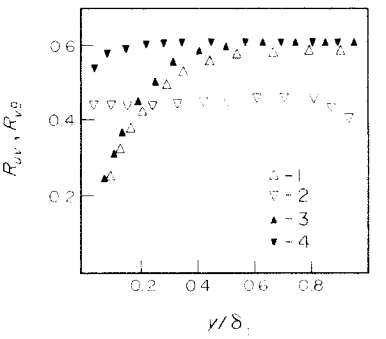

FIG. 7. Distribution of correlation coefficients: (1) $R_{\overline{uv}}$ ($b = 0.0033$, $K = 2.35 \times 10^{-6}$); (2) $R_{\overline{uv}}$ ($b = 0$, $K = 0$); (3) $R_{\overline{v\theta}}$ ($b = 0.0033$, $K = 2.35 \times 10^{-6}$); (4) $R_{\overline{v\theta}}$ ($b = 0$, $K = 0$).

A comparison of the distribution of individual components of balance equations (1)–(4) with the corresponding distributions obtained in the non-gradient region of flow allows a number of interesting conclusions.

Thus, in the cross-section of the boundary layer investigated the production of Reynolds stresses is balanced out by the terms containing pressure fluctuations actually over the entire depth of the boundary layer (Fig. 9), and this, as is known, testifies to the validity of the use of the turbulent viscosity concept. On the other hand, substantial convective and diffusive turbulent energy transfer in the wall region of the boundary layer studied (Fig. 10) points to the absence of local equilibrium and, consequently, to the necessity of the use of the turbulent energy balance equation in modelling.

Moreover, in contrast to the diffuser flow region [8], the generation of the turbulent heat flux is almost fully compensated by the terms which involve the pressure fluctuations.

The experimental data obtained made it possible to assess the validity of the currently known hypotheses used for the approximation of the pressure fluctuations—temperature fluctuation gradient correlation in the equation of turbulent heat flux transfer.

A more general approach to the modelling of this

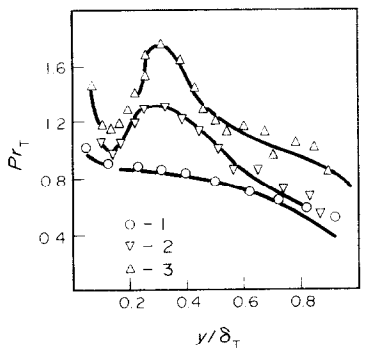

FIG. 8. Distribution of Pr_T numbers: (1) $K = 0$, $b = 0$; (2) $K = 2.35 \times 10^{-6}$, $b = 0$; (3) $K = 2.35 \times 10^{-6}$, $b = 0.0033$.

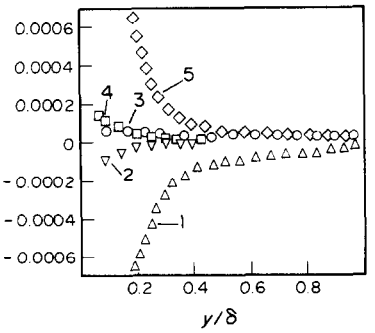

FIG. 9. Turbulent shear stress balance: (1) generation; (2) dissipation; (3) convection; (4) diffusion; (5) pressure fluctuations.

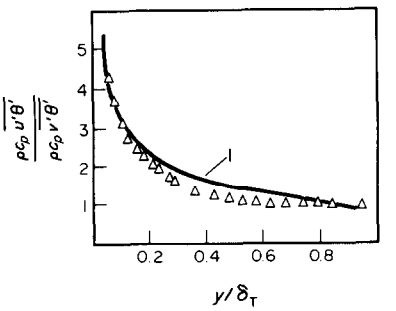

FIG. 11. The relationship between the turbulent heat fluxes: (1) calculation by equation (11).

term is that suggested by Launder and Samaraweera [11]

$$\frac{1}{\rho}\overline{p'\frac{\partial\theta'}{\partial x_i}} = \varphi_{ic_1}+\varphi_{ic_2}+\varphi_{ic_3}, \tag{5}$$

where the terms on the RHS determine the turbulent, mean-deformation and gravitational components, respectively. In the flow studied the gravitational term φ_{ic_3} can be neglected.

Following Monin [12], the quantity φ_{ic_1} is usually represented in the form

$$\varphi_{ic_1} = -C_{i_1}\left(\frac{\varepsilon}{e}\right)\overline{u_i'\theta'} \tag{6}$$

where $C_{i_1} = 2.5$–5.

Most complicated still is the account for the mean-deformation component φ_{ic_2}. Based on the symmetric shape of the two-point correlation functions, Lumly [13] has suggested the so-called 'quasi-isotropic' model

$$\varphi_{ic_2} = 0.8\,\overline{u_m'\theta'}\frac{\partial U_i}{\partial x_m} - 0.2\,\overline{u_m'\theta'}\frac{\partial U_m}{\partial x_i}, \tag{7}$$

which, for the flow in a 2-D boundary layer, takes on the form

$$\varphi^*_{ic_2} = 0.6\,\overline{v'\theta'}\frac{\partial V}{\partial y} - 0.2\,\overline{u'\theta'}\frac{\partial U}{\partial y}. \tag{8}$$

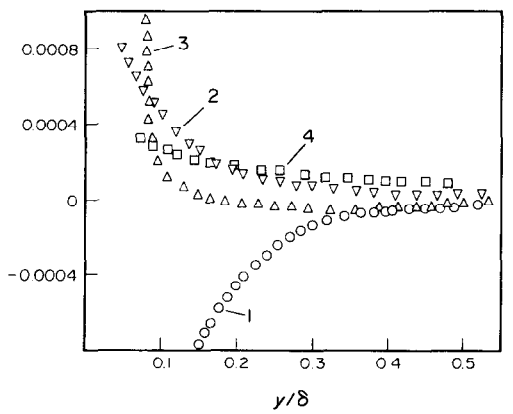

FIG. 10. Turbulent energy balance: (1) generation; (2) dissipation; (3) diffusion; (4) convection.

Launder [14], having assumed that the mean-deformation term contributes mainly to the 'destruction of production', has suggested another form of relation for φ_{ic_2}, i.e.

$$\varphi_{ic_2} = C_{i_2}\overline{u_m'\theta'}\frac{\partial U_i}{\partial x_m}, \tag{9}$$

which, under the studied flow conditions, takes the form

$$\varphi^{**}_{ic_2} = C_{i_2}\overline{v'\theta'}\frac{\partial V}{\partial y}, \tag{10}$$

where $C_{i_2} = 0.4$–0.5.

It is not difficult to see that equation (8) contains a new unknown quantity $\overline{u'\theta'}$, for the determination of which Lumly [13] has suggested the relation $\overline{u'\theta'}/\overline{v'\theta'}$ = const. However, the experimental data obtained indicate that at the cross-section of the boundary layer investigated this relation is strongly violated (Fig. 11).

However, by neglecting diffusion and convection and on having determined the quantity $\overline{u'\theta'}$ from the respective transport equation on the assumption that the mean-deformation component can be written down in the form of equation (7), one can obtain the following relation

$$\overline{u'\theta'} = \frac{1}{C_{i_1}}\frac{e}{\varepsilon}\left[\overline{u'v'}\frac{\partial T}{\partial y} + (1+C_{i_2})\overline{v'\theta'}\frac{\partial U}{\partial y}\right], \tag{11}$$

which with sufficient accuracy describes a change in the longitudinal component of the turbulent heat flux in the cross-section of the boundary layer studied (Fig. 11).

Thus, the expression for the mean-deformation component takes the form

$$\varphi^{***}_{ic_2} = 0.6\,\overline{v'\theta'}\frac{\partial V}{\partial y} - \frac{0.2}{C_{i_1}}\frac{e}{\varepsilon}\left[\overline{u'v'}\frac{\partial T}{\partial y}\frac{\partial U}{\partial y} + \overline{v'\theta'}\left(\frac{\partial U}{\partial y}\right)^2\right]. \tag{12}$$

Comparing the expressions for $\varphi^{**}_{ic_2}$ and $\varphi^{***}_{ic_2}$, it is not difficult to see that the Launder hypothesis allows only for a portion of the mean-deformation interaction obtained on the basis of the 'quasi-isotropic' model, but the final assessment of the practical utility of that or this

approximation can be made only by comparing the results of calculation with the available experimental data.

The turbulence model used in calculations was the 'e–ε' model described in detail in refs. [6, 9]. This model was augmented with the equation of turbulent heat flux transfer written in two variants differing by the form of representation of the mean-deformation term φ_{ic_2}

$$\rho U\frac{\partial\overline{v'\theta'}}{\partial x}+\rho V\frac{\partial\overline{v'\theta'}}{\partial y}=-\rho\left(\overline{u'v'}\frac{\partial T}{\partial x}+1.6\overline{u'v'}\frac{\partial T}{\partial y}\right)+\frac{\partial}{\partial y}\left[\left(\frac{\mu}{Pr}+\mu_T\right)\frac{\partial\overline{v'\theta'}}{\partial y}\right]-3.8\rho\frac{\overline{v'\theta'}}{e}\varepsilon-0.3\rho\overline{v'\theta'}\frac{e^{1/2}}{y}-0.6\overline{v'\theta'}\frac{\partial V}{\partial y},\quad(13)$$

$$\rho U\frac{\partial\overline{v'\theta'}}{\partial x}+\rho V\frac{\partial\overline{v'\theta'}}{\partial y}=-\rho\left(\overline{u'v'}\frac{\partial T}{\partial x}+1.6\overline{u'v'}\frac{\partial T}{\partial y}\right)+\frac{\partial}{\partial y}\left[\left(\frac{\mu}{Pr}+\mu_T\right)\frac{\partial\overline{v'\theta'}}{\partial y}\right]-3.8\rho\frac{\overline{v'\theta'}}{e}\varepsilon-0.3\rho\overline{v'\theta'}\frac{e^{1/2}}{y}+0.065\rho\frac{\overline{u'v'}e}{\varepsilon}\frac{\partial T}{\partial y}\frac{\partial u}{\partial y}-0.035\rho\frac{\overline{v'\theta'}e}{\varepsilon}\left(\frac{\partial U}{\partial y}\right)^2.\quad(14)$$

The coefficients which enter into equations (13) and (14) and which have been chosen as a result of computer optimization, are within the limits of values used in previous publications [11].

Comparing the results of calculations by the 'e–ε' model, augmented with the turbulent heat flux transport equation, with the experimental data (Figs. 6 and 12), it is easy to see that both versions of the calculation of the nongradient flow past a plate practically coincide.

However, in the confusor region of flow, even on an impervious surface, an insufficiently correct account for the mean-deformation component of correlation of φ_{ic_2}

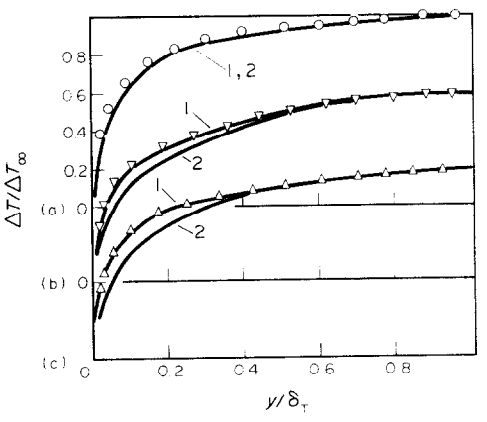

FIG. 12. Temperature distribution in a boundary layer: (a) $K = 0$, $b = 0$; (b) $K = 2.35 \times 10^{-6}$, $b = 0$; (c) $K = 2.35 \times 10^{-6}$, $b = 0.0033$; (1) calculation by equation (14); (2) calculation by equation (13).

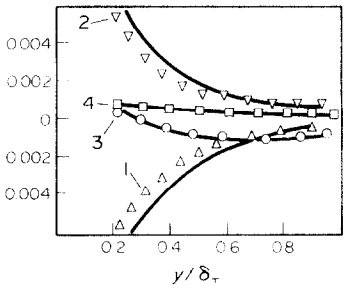

FIG. 13. Turbulent heat flux balance: (1) generation; (2) pressure fluctuations; (3) diffusion; (4) convection. Lines, calculation by equation (14).

leads to noticeable deviations between the predicted and experimental distributions of temperature and of turbulent heat flux in the cross-sections of the studied boundary layers, while equation (14) which includes the $\varphi_{ic_2}^{***}$ approximation, reproduces a rather complex pattern of experimental distributions, including the Pr_T distributions in the cross-sections of the studied wall flows (Fig. 8), all this being not by chance, since equation (14) rather well reproduces the processes of production, destruction and transport of turbulent heat flux in the cross-section of the boundary layer studied (Fig. 13).

The analysis of calculation results has shown that the 'e–ε' model augmented with equation (14), predicts the integral characteristics [including also St (Fig. 4)] which differ from the experimental ones by no more than 5%.

REFERENCES

1. A. F. Orlando, R. J. Moffat and W. M. Kays, Turbulent transport of heat and momentum in a boundary layer subject to deceleration, suction and variable wall temperature, Report HMT-17, Stanford University (1974).
2. D. G. Whitten, R. J. Moffat and W. M. Kays, Heat transfer to a turbulent boundary layer with non-uniform blowing and surface temperature, Report HMT-8, Stanford University (1969).
3. V. P. Zabolotsky, P. S. Roganov and E. V. Shishov, An experimental facility and the results of investigation of the properties of an accelerated boundary layer with suction, *Trudy MLTI* No. 138, 72–81 (1981).
4. A. I. Leontiev, E. V. Shishov and V. M. Belov, The use of a linearized hot-wire anemometer signal for the diagnosis of nonisothermal turbulent boundary layers, *Proc. 2nd All-Union Conf. on Experimental Methods and Equipment for the Investigation of Turbulence*, pp. 143–150. Novosibirsk (1977).
5. P. S. Roganov and E. V. Shishov, Experimental determination of friction on the wall in a retarded turbulent boundary layer, *Trudy MLTI* No. 112, 151–157 (1978).
6. A. I. Leontiev, E. V. Shishov, V. N. Afanasiev and V. P. Zabolotsky, The study of the fluctuational structure of a thermal turbulent boundary layer under the conditions of flow laminarization, in *Heat and Mass Transfer—6*, Vol. 1, Part 2, pp. 136–146, Minsk (1980).
7. E. V. Shishov, P. S. Roganov, V. M. Belov and V. N. Afanasiev, Experimental investigation of the turbulent

energy balance components in the cross-section of a decelerated turbulent boundary layer, *Izv. VUZov, Aviats. Tekh.* No. 3, 108–112 (1978).
8. A. I. Leontiev, E. V. Shishov and P. S. Roganov, Experimental study of turbulent energy and turbulent heat flux diffusive transport in retarded turbulent boundary layers, *2nd Symp. on Turbulent Shear Flow*, pp. 9.5–9.11. Imperial College, London (1979).
9. V. P. Zabolotsky, P. S. Roganov and E. V. Shishov, The study of the processes of turbulence transport in an accelerated turbulent boundary layer with suction, *Trudy MLTI* No. 138, 85–92 (1981).
10. E. V. Shishov, P. S. Roganov, V. N. Afanasiev and V. M. Belov, Experimental investigation of the balance of temperature fluctuations in the diffusor region of flow, *Izv. VUZov, Aviats. Tekh.* No. 3, 55–60 (1979).
11. B. Launder and D. Samaraweera, Application of a second-moment turbulence closure to heat and mass transport in thin shear flows, *Int. J. Heat Mass Transfer* **22**, 1631–1644 (1979).
12. A. S. Monin, The properties of symmetry in the atmospheric turbulence, *Izv. Akad. Nauk SSSR, Ser. Fiz. Atm. Okeana* **1**(1), 45–54 (1965).
13. J. L. Lumly, Prediction methods for turbulent flows, Lecture Series No. 76, von Karman Institute, Belgium (1975).
14. B. Launder, Scalar property transport by turbulence, Report N HTS/73/26, Dept. Mech. Engng, Imperial College, London (1973).

QUELQUES ASPECTS DU TRANSFERT THERMIQUE TURBULENT DANS DES ECOULEMENTS ACCELERES SUR DES SURFACES PERMEABLES

Résumé—On présente des résultats d'une expérimentation sur la structure et les mécanismes de transfert turbulent dans une couche limite accélérée sur une surface perméable. On analyse différentes modélisations pour un flux thermique turbulent. Une attention est portée à la modélisation des corrélations pression–température.

EINIGE ASPEKTE DES TURBULENTEN WÄRMEÜBERGANGS BEI BESCHLEUNIGTER STRÖMUNG AN PERMEABLEN WÄNDEN

Zusammenfassung—Die Ergebnisse einer experimentellen Untersuchung der Struktur und der turbulenten Transportvorgänge in einer beschleunigten Grenzschicht an einer permeablen Wand werden mitgeteilt. Es werden die Möglichkeiten, die Transportgleichung für einen turbulenten Wärmestrom zu formulieren, untersucht. Das Schwergewicht wird auf die Formulierung von Beziehungen zwischen Druck und Temperatur gelegt.

ОСОБЕННОСТИ ТУРБУЛЕНТНОГО ТЕПЛОПЕРЕНОСА В УСКОРЕННЫХ ПОТОКАХ НА ПРОНИЦАЕМЫХ ПОВЕРХНОСТЯХ

Аннотация—Представлены результаты экспериментального исследования структуры и процессов турбулентного переноса в ускоренном пограничном слое на проницаемой поверхности. Анализируются возможные пути моделирования уравнения переноса турбулентного теплового потока. Особое внимание уделено моделированию корреляции пульсаций давления и температуры.